Author's personal copy

International Journal of Multiphase Flow 37 (2011) 987–993

Contents lists available at ScienceDirect

International Journal of Multiphase Flow

journal homepage: www.elsevier.com/locate/ijmulflow

Brief communication

Three-dimensional convective and absolute instabilities in pressure-driven two-layer channel flow

K.C. Sahu [a,*], O.K. Matar [a,b]

[a] Department of Chemical Engineering, Indian Institute of Technology Hyderabad, Yeddumailaram, 502 205 Andhra Pradesh, India
[b] Department of Chemical Engineering, Imperial College London, South Kensington Campus, London SW7 2AZ, UK

ARTICLE INFO

Article history:
Received 8 February 2011
Received in revised form 10 April 2011
Accepted 2 May 2011
Available online 6 May 2011

Keywords:
Interfacial instability
Multiphase flow
Immiscible fluids
Three-dimensional disturbances
Linear stability analysis

1. Introduction

The stability of two-layer flows in planar channels and pipes has received considerable attention in the literature experimentally, theoretically and numerically. This is due to the central importance of these flows to numerous engineering applications, such as the cleaning of fast-moving consumer good plants, transportation of crude oil in pipelines (Joseph et al., 1997), mixing of liquids using centerline injectors, up-stream of static mixers (Cao et al., 2003), and the removal of highly viscous or elasto-viscoplastic material adhering to pipes by using fast-flowing water streams (Regner et al., 2007).

The instability of two-dimensional disturbances in two-fluid Poiseuille flows has been studied by many authors via linear stability analyses (Yiantsios and Higgins, 1988b; Hooper and Boyd, 1983; South and Hooper, 1999; Frigaard, 2001), with some being carried out in the long-wave limit (Yih, 1967; Yiantsios and Higgins, 1988a; Khomami, 1990a,b), as well as experimental techniques (Kao and Park, 1972). An extended review can be found in (Boomkamp and Miesen, 1996). Sahu et al. (2007) studied the linear instability of two-dimensional disturbances in a pressure-driven two-layer channel flow, wherein a Newtonian fluid layer overlies a layer of a Herschel–Bulkley fluid. Their results indicate that increasing the yield stress, prior to the formation of unyielded zones, and shear-thickening tendency are destablising. The convective and absolute nature of two-dimensional disturbances in a similar system is studied by Valluri et al. (2010). The stability maps demarcating the areas of absolute and convective instabilities as a function of other parameter values were presented. Frigaard (2001) studied the two-dimensional linear stability of two-layer Poiseuille flow of two Bingham fluids. Unlike the study of Sahu et al. (2007), the case studied by Frigaard (2001), involves an unyielded region between the Newtonian fluid and the yielded part of the Bingham fluid. Interfacial waves would not develop under such conditions; this suppression of interfacial modes then leads to super-stable two-layer flows (Frigaard, 2001). On the other hand, the effect of three-dimensional disturbances on the stability of pressure-driven channel flow, has received little attention.

Squire (1933) studied the stability of viscous fluid flow between parallel walls and found that every unstable three-dimensional disturbance is associated with a more unstable two-dimensional disturbance at a lower value of the Reynolds number. This result is commonly known as 'Squire's theorem' (Drazin and Reid, 1985) and the connection between the two- and three- dimensional disturbances is known as 'Squire's transformation'. For two superposed fluids in plane Poiseuille flow, Yiantsios and Higgins (1988a) showed that three-dimensional disturbances are associated with smaller Reynolds numbers, and larger capillary contributions and density stratifications. The larger capillary contributions are stabilising for all parameter values, as is density stratification provided the density of the upper fluid is lower than that of the lower one. Thus, although a Squire's transformation can exist for all flow parameters, a Squire's theorem can only exist provided the Reynolds

* Corresponding author.
E-mail address: ksahu@iith.ac.in (K.C. Sahu).

0301-9322/$ - see front matter © 2011 Elsevier Ltd. All rights reserved.
doi:10.1016/j.ijmultiphaseflow.2011.05.005

Author's personal copy

number has a destabilising effect. They found that in the absence of surface tension and gravitational effects, Squire's theorem is valid for $t_r > \sqrt{m}$ since the Reynolds number is destabilising; here, t_r is the thickness ratio of the two fluids and m is the viscosity ratio. For $t_r < \sqrt{m}$, the Reynolds number is stabilising and Squire's theorem no longer exists. This is also true in the presence of destabilising density stratification.

Following the remark by Yiantsios and Higgins (1988a), in the absence of a Squire's theorem it is necessary to perform a three-dimensional linear stability analysis in order to determine whether or not two-dimensional disturbances correspond to the most dangerous ones. Sahu and Hema (2011) examined the three-dimensional linear stability of two-layer plane Poiseuille flow, wherein a Newtonian fluid layer overlies a layer of a Herschel–Bulkley fluid, focussing on the range of parameters for which Squire's theorem does not exist. They demonstrated through a linear stability analysis the presence of three-dimensional instabilities. Malik and Hooper (2007) also studied the effect of three-dimensional disturbances on two-fluid channel flow, wherein both the fluids are Newtonian. Using an energy analysis they showed that maximum amplification of the disturbances is due to the "lift-up effect" as in case of single phase flow. They also found that, for some parametric regime, the maximum disturbance energy growth is associated with three-dimensional disturbances.

In this paper, a generalized linear stability analysis (Huerre and Monkewitz, 1990; Chomaz, 2005; Schmid and Henningson, 2001) (in which both the spatial wavenumber and temporal frequency are complex) of three-dimensional disturbances is carried out, which allows the demarcation of the boundaries between convectively and absolutely unstable flows in the space of relevant parameters: the Reynolds number and a viscosity ratio. To the best of our knowledge, this type of analysis, which has been performed previously for jets, mixing layers, wakes, boundary layers etc. for two-dimensional disturbances, has not been carried out for two-fluid channel flows in the context of three-dimensional disturbances.

The rest of this paper is organised as follows. Details of the problem formulation are provided in Section 2, and the results of the linear stability analysis are presented in Section 3. Concluding remarks are provided in Section 4.

2. Formulation

A pressure-driven channel flow of two immiscible Newtonian and incompressible fluids is considered. A rectangular coordinate system, (x,y,z), is used to model this flow (U_j,V_j,W_j), where x, y and z denote the streamwise, spanwise and wall normal coordinates, respectively, as shown in Fig. 1. U_j, V_j and W_j are the velocity components of fluid 'j' in the streamwise, spanwise and wall normal directions, respectively. The rigid and impermeable channel walls are located at $z = 0$ and $z = H$, respectively, and the sharp interface, which separates the immiscible fluids, is at $z = h^0$. The height of the channel, H, and $U_m \equiv Q/H$ are used as the length and velocity scales, respectively, in order to nondimensionalise the equations of motion, where Q denotes the total flow rate per unit transverse length. The viscosity and density have been scaled with μ_2 and ρ_2, respectively, such that the viscosity ratio, $m \equiv \mu_1/\mu_2$, and density ratio, $r \equiv \rho_1/\rho_2$, wherein μ_1 and ρ_1, μ_2 and ρ_2 are the viscosity and the density of the lower and upper fluids, respectively. The reduced dimensionless pressure P_j in fluid 'j' is related to the corresponding total dimensional pressure p_j through

$$P_j = \frac{H}{\mu_2 U_m}\left[p_j + \rho_j g(z-h)\right] \ (j = 1,2), \tag{1}$$

where g is the gravitational acceleration. We analyse linear stability characteristics of the base state described below.

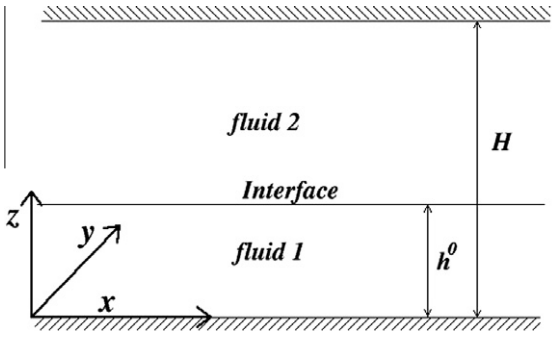

Fig. 1. Schematic of a two-layer flow in a channel of height H, where h^0 represents the thickness of the lower fluid.

2.1. Base state

The base state corresponds to a steady, parallel, fully-developed flow in both the layers separated by a flat interface, i.e., $V_j = W_j = 0$; U_j is only a function of z and pressure distribution ($P_1 = P_2 = P$) is linear in x.

$$U_1 = \frac{1}{2m}\frac{dP}{dx}\left[z^2 + \left\{\frac{h^{0^2} + m(1-h^0)}{m(h^0-1) - h^0}\right\}z\right], \tag{2}$$

$$U_2 = \frac{1}{2}\frac{dP}{dx}\left[z^2 - 1 + \left\{\frac{h^{0^2} + m(1-h^0)}{m(h^0-1) - h^0}\right\}(z-1)\right]. \tag{3}$$

The pressure gradient, dP/dx, is obtained from the constant volumetric flow rate condition, i.e.,

$$\int_0^{h^0} U_1 dz + \int_{h^0}^1 U_2 dz = 1. \tag{4}$$

We obtained Eqs. (2) and (3) by integrating the steady, fully-developed dimensionless Navier–Stokes equations, imposing the no-slip conditions at the walls and demanding continuity of velocity and the tangential component of the stress at the interface. Typical basic state profiles of the steady, streamwise velocity component for $h^0 = 0.3$ are shown in Fig. 2. These parameter values are chosen such that they satisfy $n \equiv h^0/(1-h^0) < \sqrt{m}$ for which there is no Squire's theorem (Yiantsios and Higgins, 1988a). Inspection of

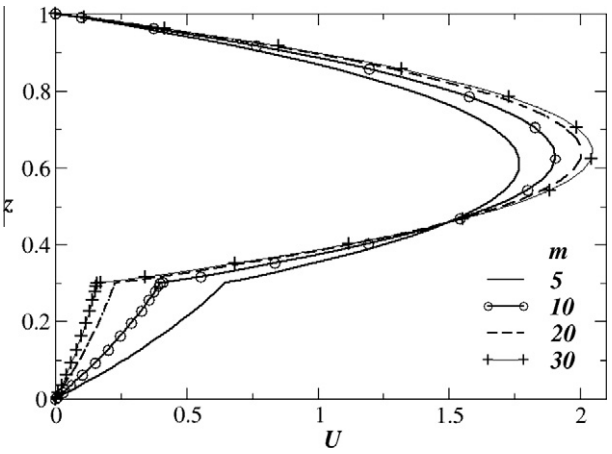

Fig. 2. Basic state profiles of the steady, streamwise velocity profiles for different viscosity ratios. The height of the interface from the bottom wall, $h^0 = 0.3$.

Author's personal copy

Fig. 2 reveals that increasing the value of m leads to an increase in maximal velocity contrast between the upper and lower fluids.

2.2. Linear stability analysis

We examine the linear stability of the base state given by Eqs. (2) and (3), to infinitesimal, three-dimensional (3D) disturbances using a normal modes analysis. Each flow variable is expressed as the sum of a base state and a 3D perturbation,

$$(\tilde{u}_j, \tilde{v}_j, \tilde{w}_j, \tilde{P}_j)(x,y,z,t) = [U_j(z), 0, 0, P_j] + (\hat{u}_j, \hat{v}_j, \hat{w}_j, \hat{p}_j)(x,y,z,t), \quad (5)$$

with $j = 1, 2$. Similarly, h can be expressed as,

$$h(x,y,t) = h^0 + \hat{h}, \quad (6)$$

where the hats designate perturbation variables. The superscript '0' designates the base state quantities. Substitution of Eqs. (5) and (6) into the governing equations followed by subtraction of the base state equations, subsequent linearization and elimination of the pressure perturbation yields linear stability equations in terms of primary variables. These equations are re-expressed in terms of the wall-normal perturbation velocity, $\hat{w}_j$, and wall-normal component of vorticity, $\hat{\eta}_j z \equiv \partial\hat{u}_j/\partial y - \partial\hat{v}_j/\partial x$, and then decomposed into an amplitude and a wave part by using a normal modes analysis:

$$(\hat{w}_j, \hat{\eta}_j, \hat{p}_j)(x,y,z,t) = (\tilde{w}_j, \tilde{\eta}_j, \tilde{p}_j)(z)\mathrm{e}^{\mathbf{i}(\alpha x+\beta y-\Omega t)},$$
$$\hat{h}(x,y,t) = \tilde{h}\mathrm{e}^{\mathbf{i}(\alpha x+\beta y-\Omega t)}, \quad i = 1,2, \quad (7)$$

where $\mathbf{i} \equiv \sqrt{-1}$, $\tilde{w}_j$, $\tilde{\eta}_j$, $\tilde{p}$ and $\tilde{h}$ denote the amplitudes of the wall-normal velocity and vorticity, pressure and interfacial perturbations, respectively; α and β denote the streamwise and spanwise wavenumbers, respectively, and $\Omega(=\alpha c)$ stands for the disturbance frequency, wherein c is the phase speed of the disturbance. This after suppressing the tilde notations, yields the following stability equations in both layers. In the lower layer:

$$\mathbf{i}\alpha r\mathrm{Re}\left[\{w_1'' - (\alpha^2+\beta^2)w_1\}(U_1 - c) - U_1''w_1\right] = m[w_1'''' - 2(\alpha^2+\beta^2)w_1'' + (\alpha^2+\beta^2)^2 w_1], \quad (8)$$

$$\mathbf{i}r\mathrm{Re}\left[\alpha\eta_1(U_1 - c) + \beta U_1' w_1\right] = m\left[\eta_1'' - (\alpha^2+\beta^2)\eta_1\right]. \quad (9)$$

In the upper layer:

$$\mathbf{i}\alpha Re\left[\{w_2'' - (\alpha^2+\beta^2)w_2\}(U_2 - c) - U_2''w_2\right] = w_2'''' - 2(\alpha^2+\beta^2)w_2'' + (\alpha^2+\beta^2)^2 w_2, \quad (10)$$

$$\mathbf{i}Re\left[\alpha\eta_2(U_2 - c) + \beta U_2' w_2\right] = \eta_2'' - (\alpha^2+\beta^2)\eta_2. \quad (11)$$

Solutions of these equations are then subject to the following boundary conditions: no-slip and no-penetration conditions at the walls can be written as

$$w_1 = w_1' = \eta_1 = 0 \quad \text{at} \quad z = 0, \quad (12)$$
$$w_2 = w_2' = \eta_2 = 0 \quad \text{at} \quad z = 1. \quad (13)$$

The kinematic boundary condition gives

$$h = \frac{w_1}{\mathbf{i}\alpha(U_1 - c)} = \frac{w_2}{\mathbf{i}\alpha(U_2 - c)}. \quad (14)$$

Conditions of continuity of the velocity in the streamwise, spanwise and normal directions at the interface are expressed as,

$$w_1' - \mathbf{i}\alpha h U_1' = w_2' - \mathbf{i}\alpha h U_2', \quad (15)$$
$$\eta_1 + \mathbf{i}\beta h U_1' = \eta_2 + \mathbf{i}\beta h U_2', \quad (16)$$
$$w_1 = w_2. \quad (17)$$

The normal stress jump and continuity of the tangential stress balance in the streamwise and spanwise directions are respectively given by

$$\mathbf{i}\alpha Re\left[r\{w_1'(c - U_1) + U_1' w_1\} - \{w_2'(c - U_2) + U_2' w_2\}\right] + m\left[w_1''' - 3(\alpha^2+\beta^2)w_1'\right] - w_2''' + 3(\alpha^2+\beta^2)w_2' = (\alpha^2+\beta^2)\{\Gamma(\alpha^2+\beta^2) + G\}\frac{(w_2' - w_1')}{\mathbf{i}\alpha(U_2' - U_1')}, \quad (18)$$

$$m\left[w_1'' + (\alpha^2+\beta^2)w_1\right] - \frac{(mU_1'' - U_2'')}{(U_1 - c)}w_1 = w_2'' + (\alpha^2+\beta^2)w_2, \quad (19)$$

$$\mu_1^0\eta_1' + \mathbf{i}\beta\mathscr{S}U_1'\pi + \frac{(\mu_1^0 U_1'' - U_2'')}{\alpha(U_1 - c)}\beta w_1 = \eta_2'. \quad (20)$$

We confirm that Eqs. (8)–(11) along with the boundary conditions (12)–(20) constitute an eigenvalue problem. Here, the primes represent differentiation with respect to z, Re ($\equiv\rho_2 U_m H/\mu_2$) is the Reynolds number, $G \equiv (\rho_1 - \rho_2)g\ H^2/\mu_2 U_m$ is a dimensionless gravitational parameter, and $\Gamma \equiv \gamma/\mu_2 U_m$ is an inverse capillary number, in which γ denotes the interfacial tension.

The linear stability equations, Eqs. (8)–(11), are the same as the Orr-Sommerfeld and Squire equations for a Newtonian fluid as given in Schmid and Henningson (2001). Our stability equations and the boundary conditions match those of Sahu and Hema (2011) and Nouar et al. (2007) for a Newtonian fluid. The existence of the eigenfunctions, (w_1, η_1) and (w_2, η_2) corresponding to the intervals $[0 - h^0]$ and $[h^0 - 1]$, respectively, is contingent upon α and Ω satisfying a dispersion relation, $D(\alpha, \beta, \Omega;\ m, r, Re, G, \Gamma)$. In cases, wherein Ω is complex (real) and α and β are real (complex), the modes are *temporal* (*spatial*). In order to determine whether the flow is stable or unstable, and, in the latter case, whether *absolutely* or *convectively* unstable, we follow an approach, which has been used previously to analyze the stability of mixing layers, jets and wakes, and in plasma flows (Briggs, 1964; Bers, 1983; Huerre and Monkewitz, 1990; Vihinen et al., 1997; Criminale et al., 2003; Chomaz, 2005; Kaiktsis and Monkewitz, 2003). Previously, we had also applied this approach to analyse convective-absolute instabilities in miscible two-layer channel flow (Sahu et al., 2009). The procedure is briefly outlined below.

The linearised differential operator is first associated with a dispersion relation in complex (Ω, α) space for finite β values. Then, one introduces a Green's function, $G(x,y,t)$, in order to represent the response of the linearised system to an impulse perturbation. The method of steepest descent is then used to study the long-time behaviour of G along different 'rays'; the latter correspond to constant values of x/t. This method leads to the saddle point condition

$$\frac{\partial\Omega}{\partial\alpha}(\alpha) = \frac{x}{t}, \quad (21)$$

which is real and corresponds to the group velocity. For flow *instability*, one must have $\Omega_{i,max} > 0$, i.e. the maximum temporal growth rate, which corresponds to Im (Ω), must be positive. Here, $\Omega_{i,max} = \Omega_i(\alpha_{max})$ and satisfies $\partial\Omega_i/\partial\alpha(\alpha_{max}) = 0$ in which α_{max} is real and is referred to below as the 'most dangerous mode'. In order to determine whether the flow is *convectively* or *absolutely* unstable, one calculates the so-called "absolute frequency", $\Omega_0 = \Omega(\alpha_0)$; here, the "absolute wavenumber", α_0, may be complex and satisfies

$$\frac{\partial\Omega}{\partial\alpha}(\alpha_0) = 0. \quad (22)$$

Comparison of Eq. (22) with Eq. (21) reveals that the former corresponds to the ray $x/t = 0$ representing the zero group velocity. If Im $(\Omega_0) \equiv \Omega_{0,i} > 0$, that is if the "absolute growth rate" is positive, then

Author's personal copy

an impulse disturbance grows locally and spreads both upstream and downstream from its source, and the flow is said to be *absolutely* unstable. If $\Omega_{0,i} < 0$ then impulse disturbances grow downstream from their source only giving rise to a *convectively* unstable flow.

2.3. Numerical procedure

This eigenvalue problem (Eq. (8)–(20)) is solved using the public domain software, LAPACK, and the Chebyshev spectral collocation method (Canuto et al., 1987). We have checked the dependence of our numerical solutions upon mesh refinement by considering different values of the order of Chebyshev polynomials, N, and found that results are indistinguishable for $N > 51$ (not shown); thus, $N = 81$ is used to generate the rest of the results. Our results are also in excellent agreement with those of Sahu and Hema (2011), South and Hooper (1999) and Yiantsios and Higgins (1988a).

3. Results and discussion

We begin the presentation of our results by plotting the numerically-generated dispersion curves corresponding to the variation of the growth rate, Ω_i, with β for different values of α in Fig. 3. Here, Ω_i has been normalised by Ω_{2D}, the value of Ω_i associated with two-dimensional disturbance ($\beta = 0$), for each value of α used. The rest of the parameter values are $Re = 500$, $\Gamma = 0.01$, $G = 10$, $m = 30$, $r = 1.2$ and $h^0 = 0.3$. It can be seen that the dispersion curves exhibit a well-defined maximum associated with a finite β value for an intermediate value of α, $\alpha \approx 0.75$, and 'cut-off' modes, for which $\Omega_i/\Omega_{2D} < 1$, for large β values. Close inspection of Fig. 3 reveals that the β values associated with the maximal normalised growth rates and the 'cut-off' mode increase with increase in the value of α for $\alpha \leqslant 0.75$, then decrease for $\alpha > 0.75$. Thus, the results depicted in Fig. 3 demonstrate that the temporal linear instabilities accompanying the flow for this set of parameters are three-dimensional.

In order to identify the physical mechanism and the nature of unstable modes, we perform an energy budget analysis (Govindarajan et al., 2001; Boomkamp and Miesen, 1996). The energy equation is derived by taking the inner product of the horizontal and vertical components of the Navier–Stokes equations with their respective velocity components. The resultant equation is decomposed into energy production and dissipation terms, and averaged over the wavelengths, $2\pi/\alpha$ and $2\pi/\beta$, in the x and y directions, respectively, and then integrated over the height of channel. This decomposition allows one to isolate the mechanisms by which energy is transferred from the base flow to the disturbances and also to determine the type of instability mode, whether 'interfacial' or 'shear'. A similar analysis was performed recently by Sahu et al. (2007, 2009) and Selvam et al. (2007) for immiscible non-Newtonian, miscible channel flows and miscible core annular flows, respectively.

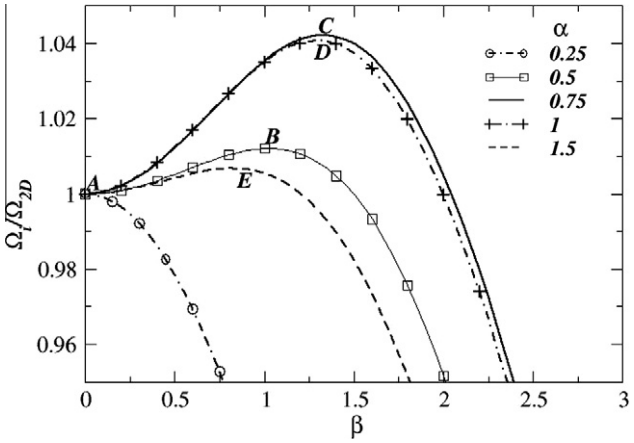

Fig. 3. The dispersion curves (Ω_i/Ω_{2D} vs. β) for different value of α. The rest of the parameter values are $Re = 500$, $h^0 = 0.3$, $m = 30$, $r = 1.2$, $\Gamma = 0.01$ and $G = 10$.

$$\sum_{j=1}^{2} KIN_j = \sum_{j=1}^{2} DIS_j + \sum_{j=1}^{2} REY_j + INT, \tag{23}$$

where subscript $j = 1$ and $j = 2$ represent the lower and upper fluids, respectively. In Eq. (23), KIN_j, DIS_j and REY_j are expressed by

$$KIN_j = \frac{r_j}{\lambda_1\lambda_2}\frac{\mathrm{d}}{\mathrm{d}t}\int_{a_j}^{b_j}\mathrm{d}z\int_0^{\lambda_2}dy\int_0^{\lambda_1}\mathrm{d}x\left[\frac{1}{2}\left(\hat{u}_j^2+\hat{v}_j^2+\hat{w}_j^2\right)\right], \tag{24}$$

$$\begin{aligned} DIS_j = -\frac{1}{\lambda_1\lambda_2 Re}\int_{a_j}^{b_j}dz\int_0^{\lambda_2}dy\int_0^{\lambda_1}\mu_j\mathrm{d}x\Bigg[&2\left(\frac{\partial\hat{u}_j}{\partial x}\right)^2+2\left(\frac{\partial\hat{v}_j}{\partial y}\right)^2\\ &+2\left(\frac{\partial\hat{w}_j}{\partial z}\right)^2+\left(\frac{\partial\hat{u}_j}{\partial z}+\frac{\partial\hat{w}_j}{\partial x}\right)^2+\left(\frac{\partial\hat{u}_j}{\partial y}+\frac{\partial\hat{v}_j}{\partial x}\right)^2\\ &+\left(\frac{\partial\hat{v}_j}{\partial z}+\frac{\partial\hat{w}_j}{\partial y}\right)^2\Bigg], \end{aligned} \tag{25}$$

$$REY_j = \frac{r_j}{\lambda_1\lambda_2}\int_{a_j}^{b_j}\mathrm{d}z\int_0^{\lambda_2}dy\int_0^{\lambda_1}\mathrm{d}x\left[-\hat{u}_j\hat{w}_j\frac{\partial U_j}{\partial z}\right]; \tag{26}$$

for the lower fluid, $\mu_1 = m$, $r_1 = r$, $a_1 = 0$, $b_1 = h$ and for the upper fluid, $\mu_2 = 1$, $r_2 = 1$, $a_2 = h$, $b_2 = 1$. KIN_j represents the spatially averaged rate of change of disturbance kinetic energy and is proportional to the growth rate. DIS_j represents the viscous dissipation of energy and is always negative. $INT = NOR + TAN$ is associated with the existence of an interface and is decomposed into NOR and TAN, the work done by the velocity and stress disturbances in the directions normal and tangential to the interface, respectively. NOR is given by

$$NOR = \frac{1}{\lambda_1\lambda_2 Re}\int_0^{\lambda_2}dy\int_0^{\lambda_1}\mathrm{d}x\left[\hat{w}_1\tau_1^{zz}-\hat{w}_2\tau_2^{zz}\right]_h^0, \tag{27}$$

which is further decomposed into TEN and HYD, work done against the deformation of the interface due to interfacial tension and gravity respectively:

$$NOR \equiv TEN + HYD, \quad \text{where} \tag{28}$$

$$TEN = \frac{1}{\lambda_1\lambda_2 Re}\int_0^{\lambda_2}dy\int_0^{\lambda_1}\mathrm{d}x\left[\hat{w}\Gamma\left(\hat{h}_{xx}+\hat{h}_{yy}\right)\right]_{z=h}, \quad \text{and} \tag{29}$$

$$HYD = \frac{1}{\lambda_1\lambda_2 Re}\int_0^{\lambda_2}dy\int_0^{\lambda_1}\mathrm{d}x\left[\hat{w}G\hat{h}\right]_{z=h}. \tag{30}$$

TAN is also further decomposed into TAN_x and TAN_y, work done by the velocity and stress disturbances in the streamwise and spanwise directions, respectively:

$$TAN_x = \frac{1}{\lambda_1\lambda_2 Re}\int_0^{\lambda_2}dy\int_0^{\lambda_1}\mathrm{d}x\left[\hat{u}_1\tau_1^{xz}-\hat{u}_2\tau_2^{xz}\right]_h, \tag{31}$$

$$TAN_y = \frac{1}{\lambda_1\lambda_2 Re}\int_0^{\lambda_2}dy\int_0^{\lambda_1}\mathrm{d}x\left[\hat{v}_1\tau_1^{yz}-\hat{v}_2\tau_2^{yz}\right]_h. \tag{32}$$

In Eqs. (27), (31) and (32) the components of stress tensor are defined as

Author's personal copy

$$\tau_j^{xz} = \mu_j\left(\frac{\partial \hat{u}_j}{\partial z} + \frac{\partial \hat{w}_j}{\partial x}\right), \quad \tau_j^{yz} = \mu_j\left(\frac{\partial \hat{v}_j}{\partial z} + \frac{\partial \hat{w}_j}{\partial y}\right), \quad \text{and}$$
$$\tau_j^{zz} = -\hat{p}_j + 2\mu_j \frac{\partial \hat{w}_j}{\partial z}. \tag{33}$$

The energy 'budgets' associated with the points labelled *A*, *B*, *C*, *D* and *E* (the maxima in the dispersion curves) in Fig. 3 are given in Table 1. The figures in Table 1 represent the contribution arising from each term in Eq. (23) scaled by the total spatially-averaged rate of change of disturbance kinetic energy, *KIN*. The energy decomposition reveals that TAN_x provides the largest positive contribution to *KIN*. Thus the unstable modes examined are all of the 'interfacial' type, and, in this case, are driven by viscosity stratification. In general, an 'interfacial' mode appears due to the presence of an interface between two immiscible fluids, which is characterised by a sudden change in fluid properties, like viscosity, or density. This mode is known to be unstable at finite Reynolds number. A simple explanation of the mechanism underlying this viscosity-stratification-driven instability for the case of two unbounded fluids is given by Hinch (1984), that has been discussed below. The other positive, albeit smaller, contribution to *KIN* for this set of parameters is due to the Reynolds stress in the upper fluid, REY_2. The dissipative terms, DIS_1 and DIS_2 provide negative contributions; this indicates that viscous dissipation provides a restoring effect and is stabilising, as expected. TAN_y is also negative for this set of parameters. It can be seen that increasing α increases REY_2 for the range of α values considered. It can also be seen that for this set of parameter values, the negative contribution to *KIN* by the total dissipative energy decreases with increasing α, reaching a minimum for $\alpha \approx 0.75$; a further increase in α values leads to a rapid increase in the negative contribution to *KIN* by the total dissipative energy. This may provide an explanation for the nonmonotonic dependence on α shown in Fig. 3. The Reynolds stress term associated with the lower fluid, REY_1, makes a negligible contribution to *KIN*.

As discussed in Section 2.2, for a given set of parameters, the value of $\Omega_{0,i}$ corresponds to a saddle point in the complex $\alpha(\equiv\alpha_r + \mathbf{i}\alpha_i)$-plane. The process of identifying $\Omega_{0,i}$ is illustrated in Fig. 4; the isocontours of Ω_r and Ω_i for $\beta = 2$ are shown in Fig. 4a and b, respectively. The rest of the parameter values are the same as those used to generate Fig. 3. It can be seen that $\Omega_0 = 2.5821 + 0.3864\mathbf{i}$, thus $\Omega_{0,i} > 0$ indicating that the absolute growth rate is positive and the flow is absolutely unstable for this set of parameters. It is also worth mentioning that our results (not shown) for two-dimensional disturbance ($\beta = 0$) are in agreement with those of Valluri et al. (2010).

Adopting a similar procedure to that employed in generating Fig. 4, the boundary in *m*-*Re* space delineating the presence of convective and absolute instabilities is calculated for different values of β and shown in Fig. 5a. The rest of the parameter values are the same as those used to generate Fig. 3. The base flow is absolutely unstable for the parameters above the curves in Fig. 5a. The slope of the curves decreases sharply with increasing *Re* reaching a minimum, Re_m, before increasing again at relatively high *Re*. Thus, absolute instabilities appear to be present in this system over an intermediate range of *Re* values. For relatively low *Re*, a large degree of viscosity stratification is required for absolute instability, whereas increasing the level of inertial contribution renders the flow convectively unstable for sufficiently large *Re*. It can also be seen in Fig. 5a that increasing the value of β leads to a decrease in the size of the region in *m*-*Re* space in which the flow is absolutely unstable. A similar increase in β also results in a decrease

Table 1
Energy 'budgets' for the points labelled *A*, *B*, *C*, *D* and *E* in Fig. 3.

Point	REY_1	REY_2	DIS_1	DIS_2	TAN_x	TAN_y	*TEN*	*HYD*
A	0	0.0043	−0.0066	−0.0298	1.0322	0	0	0
B	0	0.0198	−0.0037	−0.0326	1.0253	−0.0088	0	0
C	0	0.0295	−0.0064	−0.0319	1.0205	−0.0148	0	0
D	0	0.0372	−0.0094	−0.0307	1.0216	−0.0188	0	0
E	0	0.0477	−0.0151	−0.0279	1.0153	−0.0201	0	0.0001

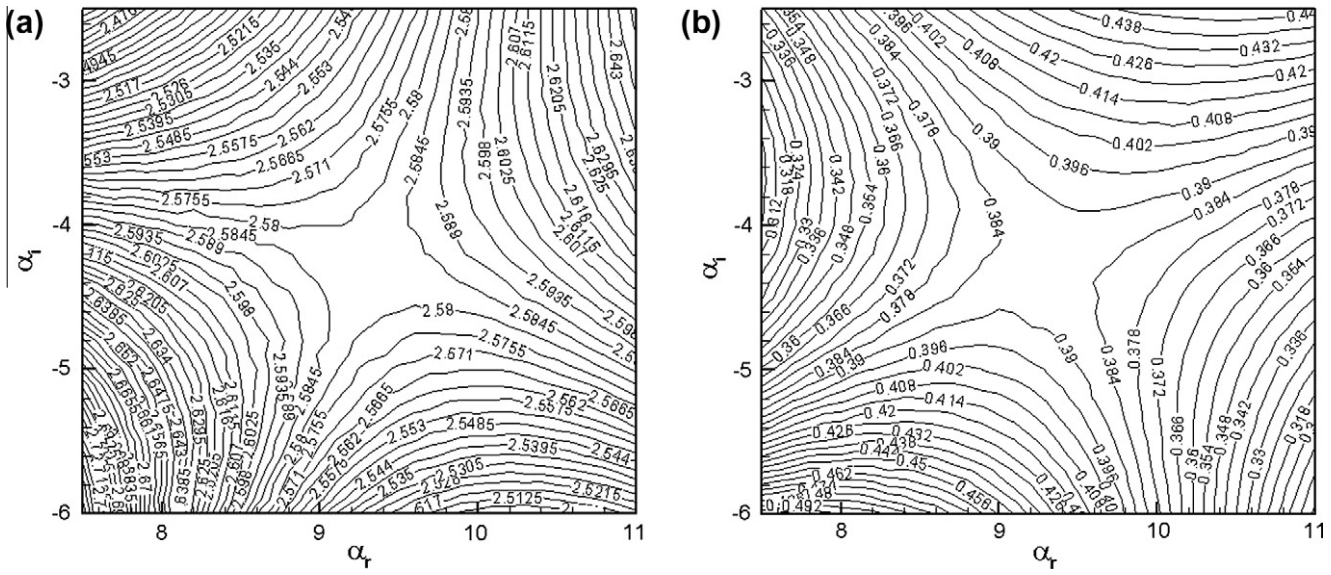

Fig. 4. Isocontours of (a) Ω_r and (b) Ω_i in the complex wave number plane. The rest of the parameter values are the same as those used to generate Fig. 3. The value of Ω at the saddle point is $2.5821 + 0.3864\mathbf{i}$.

Author's personal copy

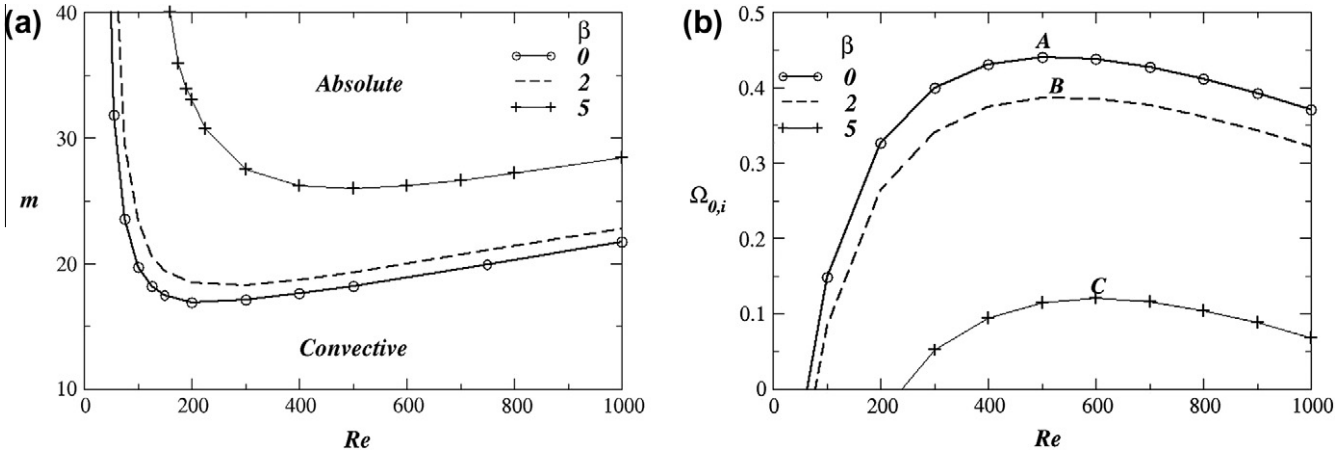

Fig. 5. (a) Stability diagram showing the regions of convective and absolute instability in *m-Re* space for different β values. (b) The variation of maximum growth rate of the absolute instability with *Re*. The rest of the parameter values are the same as those used to generate Fig. 3.

in the absolute growth rate, $\Omega_{0,i}$, as shown in Fig. 5b, which shows the variation of $\Omega_{0,i}$, with *Re* with the rest of the parameter values remaining unchanged from those used to generate Fig. 3. Inspection of Fig. 5b also shows that the maximum value of $\Omega_{0,i}$ occurs for $\beta = 0$, that is, for two dimensional disturbances. Thus, although three-dimensional disturbances are temporally more unstable than the two-dimensional disturbances for the parameter values investigated in Fig. 3, the growth rates of two-dimensional absolute instabilities is larger than those of three-dimensional ones. Thus, it is possible that for parameter values for which absolute instabilities occur, the two-dimensional modes are more likely to dominate the flow near onset than their three-dimensional counterparts.

The energy 'budgets' associated with the points labelled *A*, *B* and *C* in Fig. 5b are given in Table 2. This energy decomposition reveals that the largest contribution to *KIN* is due to TAN_x, confirming the most dangerous mode to be of 'interfacial' type. It can be seen that although increasing β increases REY_2, the negative contribution to *KIN* by the total dissipative energy also increases rapidly; hence, overall this has a stabilising influence.

Hinch (1984) shows that for the case of two unbounded fluids, of different viscosity, undergoing simple shear flow, an interfacial disturbance induces velocity perturbations that lead to positive and negative vorticity in elevated and depressed regions, respectively. For finite inertia, advection of these vortices leads to pairs of counter-rotating vortices on either side of the interface: the one in the less viscous fluid transports fluid from the depressed to the elevated regions, and is therefore destabilising; the one in the more viscous fluid, acts in the opposite direction and is stabilising. The vorticity in the less viscous fluid, however, is stronger, and therefore the instability grows, becoming more pronounced with increasing viscosity contrast.

It is difficult, however, based on the foregoing to rationalise the results shown in Fig. 5a. One may expect that for sufficiently large Reynolds numbers, sufficient advection results in large disturbance growth rates, resulting in perturbation amplification local to the source of instability, i.e. absolute instability. If the Reynolds numbers are too small or too large, then either the perturbation must advect prior to growth, or the advection rate exceeds that of perturbation growth; both of these scenarios lead to convectively unstable flows.

Table 2
Energy 'budgets' for the points labelled *A*, *B* and *C* in Fig. 5b.

Point	REY_1	REY_2	DIS_1	DIS_2	TAN_x	TAN_y	*TEN*	*HYD*
A	0	0.0097	−0.013	−0.0178	1.0211	0	0	0
B	0	0.01	−0.0134	−0.0182	1.0223	−0.0008	0	0
C	0	0.0129	−0.0154	−0.02	1.0265	−0.0039	0	0

4. Concluding remarks

We have investigated the three-dimensional convective and absolute linear instabilities in a pressure-driven two-layer channel flow, focussing on the range of parameters for which Squire's theorem does not exist. In order to examine the stability characteristics of the flow, we have derived modified Orr-Sommerfeld and Squire equations in each layer, which constitute an eigenvalue problem, wherein the complex growth rate is the eigenvalue; the streamwise and spanwise wavenumbers is taken to be complex. A Briggs-type analysis was then carried out to delineate the boundaries between linear convective and absolute instability in *m-Re* space. We have found that although three-dimensional disturbances are temporally more unstable than two-dimensional perturbations, for parameter ranges in which absolute instabilities exist, the growth rates of two-dimensional modes exceeds those of three-dimensional ones. An energy 'budget' analysis shows that the most dangerous modes are 'interfacial' ones. These results may be of particular interest to researchers studying the transient growth of the disturbances and their nonlinear evolution in two-fluid flows.

Acknowledgements

KS would like to acknowledge the support of the Indian Institute of Technology Hyderabad, India. OKM also acknowledges the support of the Technology Strategy Board of the UK through Grant No. TP//ZEE/6/1/21191.

References

Bers, A., 1983. Space-time evolution of plasma instabilities – absolute and convective. In: Rosenbluth, M.N., Sagdeev, R.Z. (Eds.), Handbook of Plasma Physics, vol. 1. North-Holland Publishing Company, Amsterdam, Amsterdam: North Holland, pp. 451–517.

Boomkamp, P.A.M., Miesen, R.H.M., 1996. Classification of instabilities in parallel two-phase flow. Int. J. Multiphase Flow 22, 67.

Briggs, R.J., 1964. Research Monograph No. 29. MIT Press, Cambridge.

Canuto, C., Hussaini, M.Y., Quarteroni, A., Zang, T., 1987. Spectral Methods in Fluid Dynamics, 1st ed. Springer-Verlag, Amsterdam.

Author's personal copy

Cao, Q., Ventresca, L., Sreenivas, K.R., Prasad, A.K., 2003. Instability due to viscosity stratification downstream of a centreline injector. Can. J. Chem. Eng. 81, 913.
Chomaz, J.-M., 2005. Global instabilities in spatially developing flows: non-normality and nonlinearity. Ann. Rev. Fluid Mech. 37, 357–392.
Criminale, W.O., Jackson, T.L., Roslin, R.D., 2003. Theory and Computation of Hydrodynamic Stability. Cambridge University Press, Cambridge, UK.
Drazin, P.G., Reid, W.H., 1985. Hydrodynamic Stability. Cambridge University Press, Cambridge.
Frigaard, I.A., 2001. Super-stable parallel flows of multiple visco-plastic fluids. J. Non-Newt. Fluid Mech. 100, 49–76.
Govindarajan, R., L'vov, S.V., Procaccia, I., 2001. Retardation of the onset of turbulence by minor viscosity contrasts. Phys. Rev. Lett. 87, 174501.
Hinch, E.J., 1984. A note on the mechanism of the instability at the interface between shearing fluids. J. Fluid Mech. 144, 463–465.
Hooper, A.P., Boyd, W.G.C., 1983. Shear flow instability at the interface between two fluids. J. Fluid Mech. 128, 507.
Huerre, P., Monkewitz, P.A., 1990. Local and global instability in spatially developing flows. Ann. Rev. Fluid Mech. 22, 473–537.
Joseph, D.D., Bai, R., Chen, K.P., Renardy, Y.Y., 1997. Core-annular flows. Ann. Rev. Fluid Mech. 29, 65.
Kaiktsis, L., Monkewitz, P.A., 2003. Global destabilization of flow over a backward-facing step. Phys. Fluids 15 (12), 3647–3658.
Kao, T.W., Park, C., 1972. Experimental investigations of the stability of channel flows. Part 2. Two-layered co-current flow in a rectangular channel. J. Fluid Mech. 52, 401–423.
Khomami, B., 1990a. Interfacial stability and deformation of two stratified power-law fluids in plane poiseuille flow. Part I. Stability analysis. J. Non-Newt. Fluid Mech. 36, 289–303.
Khomami, B., 1990b. Interfacial stability and deformation of two stratified power-law fluids in plane poiseuille flow. Part II. Interface deformation. J. Non-Newt. Fluid Mech. 37, 19–36.
Regner, M., Henningsson, M., Wiklund, J., Östergren, K., Trägårdh, C., 2007. Predicting the displacement of yoghurt by water in a pipe using CFD. Chem. Eng. Technol. 30, 844–853.
Malik, S.V., Hooper, A.P., 2007. Three-dimensional disturbances in channel flows. Phys. Fluids 19, 052102.
Nouar, C., Kabouya, N., Dusek, J., Mamou, M., 2007. Modal and non-modal linear stability of the plane Bingham–Poiseuille flow. J. Fluid Mech. 577, 211–239.
Sahu, K.C., Ding, H., Valluri, P., Matar, O.K., 2009. Linear stability analysis and numerical simulation of miscible channel flows. Phys. Fluids 21, 042104.
Sahu, K.C., Matar, O.K., 2011. Three-dimensional linear instability in pressure-driven two-layer channel flow of a newtonian and a Herschel–Bulkley fluid. Phys. Fluids 22, 112103.
Sahu, K.C., Valluri, P., Spelt, P.D.M., Matar, O.K., 2007. Linear instability of pressure-driven channel flow of a newtonian and Herschel–Bulkley fluid. Phys. Fluids 19, 122101.
Schmid, P.J., Henningson, D.S., 2001. Stability and Transition in Shear Flows. Springer, New York.
Selvam, B., Merk, S., Govindarajan, R., Meiburg, E., 2007. Stability of miscible core-annular flows with viscosity stratification. J. Fluid Mech. 592, 23–49.
South, M.J., Hooper, A.P., 1999. Linear growth in two-fluid plane Poiseuille flow. J. Fluid Mech. 381, 121–139.
Squire, H.B., 1933. On the stability for three-dimensional disturbances of viscous fluid flow between parallel walls. Proc. Roy. Soc. Lond. Ser. A 142, 621–628.
Valluri, P., Naraigh, L.O., Ding, H., Spelt, P.D.M., 2010. Linear and nonlinear spatio-temporal instability in laminar two-layer flows. J. Fluid Mech. 656, 458–480.
Vihinen, I., Honohan, A.M., Lin, S.P., 1997. Image of absolute instability in a liquid jet. Phys. Fluids 9 (11), 3117–3119.
Yiantsios, S.G., Higgins, B.G., 1988a. Linear stability of plane Poiseuille flow of two superposed fluids. Phys. Fluids 31, 3225–3238.
Yiantsios, S.G., Higgins, B.G., 1988b. Numerical solution of eigenvalue problems using the compound matrix-method. J. Comput. Phys. 74, 25.
Yih, C.S., 1967. Instability due to viscous stratification. J. Fluid Mech. 27, 337.